Egyptian Journal of Chemistry

http://ejchem.journals.ekb.eg/

Synthesis of Cobalt and Tungestin catalysts for Cracking in a Fischer-Tropsch model using Triisopropylbenzene and Dodecane as Chemical Probes

Badawy W M[1]*, S . M . Dessouky [1], Tarek M. Aboul-Fotouh[2], Mohamed A. Betiha[1], Masoud A. El-Shafie[2]

[1] Production Department, Egyptian Petroleum Research Institute (ERRI), B. O. 11727, Cairo, Egypt
[2] Mining and Petroleum Engineering Department, Faculty of Engineering, Al-Azhar University, Cairo, Egypt
Corresponding author email: leely_badawy@yahoo.com

Abstract

In this paper, three different catalysts based on the effective element concentration, cobalt substituted heteropoly acid($H_8P_2W_{17}O_{61}Co(H_2O).16\ H_2O$),were impregnated on mesoporous silica with different concentrations of Cobalt High Performane Alloy (CoHPA). The concentrations of these catalysts were as following: 5%CoHPA, 10%CoHPA, and 15%CoHPA. Mesoporous silicate is manufactured from silica that extracted from rice husk. The three catalysts have been characterized using low and high X-Ray Diffractometer(XRD), Brunauer–Emmett–Teller (BET), temperature-programmed desorption of ammonia (NH_3-TPD),pyridine-FTIR and Fourier- Transform Infrared Spectroscopy (FTIR). Triisopropylbenzene (TIPB) and dodecane (as a Fischer-Troupsch product) were used as chemical probes to identify the type of acid sites and the thermal catalytic cracking. Based on the hydrogen acceptor or hydrogen donor number (brønsted and Lewis acid sites) on the surface of the CoHPA catalyst, it was found that CoHPA catalysts have good progress in catalytic cracking byenriching catalyst surface with active acid sites. Although the catalyst already contains both acid sites, the amount of Lewis acidity increases with the increase in the tolerance of the active phase (cobalt substituted phosphotungstic acid). The results of this research work showed that the 15%CoHPA catalyst achievea TIPB cracking capacity of 51.79%. Also, the formation of moderate carbon on thiscatalyst's surface (2.6%) occurred within the good selectivity of propene by enriching the surface with Brønsted acid site. The 10%CoHPA catalyst achieved a dodecane cracking (89.3 %) at 550 °C with high selectivity to olefins (ethylene, propylene, and butene).

1. Introduction

The National Institute of Statistics and Economics (INSEE) reported that the massive increase in the world's population to more than three times over the past half-century has led to a growing demand for energy and increased consumption [1]. Over recent years, development has occurred in light and heavy crude catalytic cracking in the petroleum industry [2, 3]. The term petroleum cracking is often

_____

used in processes that break down the high molecular weight organic molecules into simple hydrocarbon molecules under high pressure and temperature [4].The cracking process of organic compounds can be accomplished in two ways; thermal or catalytic. The first involves using high temperatures to convert large hydrocarbons into very small ones, while the latter involves using catalysts with known properties to ensure the selectivity of the resulting hydrocarbons and reduce the temperature and pressure used [5].The use of catalysts in various chemical processes reduces the activation energy required to reach the desired products by providing an alternate reaction pathway. The choice of catalysts in the cracking processes of hydrocarbons is one of the most important factors. For example, the pores of the catalyst must match the hydrocarbons kinetics, the acidity must be appropriate, and have high chemical stability.

Zeolite is one of the most widely used porous solid classes in the energy field. Zeolites are solid acid catalysts composed of aluminosilicate crystals. Zeolite has been used in many industrial processes, especially petrochemical conversion, such as fluid catalytic cracking, alkylation, and isomerization, due to the high hydrothermal stability, high surface area, strong acidity and pore shape selectivity [6]. Although zeolite compounds are the most prevalent, they suffer from some drawbacks, as their micropores limit their absolute superiority over their solid acid counterparts. These micropores limit reactant molecules' arrival from reaching the active sites, particularly in reactions involving bulky molecules (low rate of access of molecules), in the zeolite crystals, and having unwanted adsorption of reactants or products during a catalytic reaction [7, 8]. Therefore, academics have tried to overcome the disadvantages of zeolite, especially the accessibility issue and diffusion limitation, to maintain or improve its catalytic activity [9-16].

M41S materials exhibited uniform pores in a size range of 2-15 nm and easy-to-control pore sizes; however, their chemical properties (acidity and hydrothermal stability) did not qualify them to replace zeolite catalysts in the petrochemical and refining industries [7, 17]. Some studies reported that treating MCM-41 with alkaline solutions increased its acidity, but this treatment damaged its uniform sieve molecular structure. There have been other attempts to enhance the acidity of MCM-41 by introducing some metals (Al, Fe, Zr, Cu, Zn, etc.), and they showed good catalytic results [15, 18-21]. The good dispersion of metallic atoms in the structure of MCM-41 is the most important factor in determining the strength, type, and number of acidities [22]. It is possible to replace some silica atoms with other metal atoms in two ways, one of which is post-

synthesis, in which the MCM-41 material binds to the metal atoms on their wall and surface by electrostatic forces and results in relatively low acidity. Also, these metals can be leached from the surface during the catalytic reaction. The other is direct synthesis, in which metal atoms incorporate into the silica structure by replacing the silica atom with the metal during the synthesis process. This method leads to an excellent dispersion of the metal atoms in the silica structure, which was reflected by an increase in the acidity's strength and the number of acid sites [23, 24]. Moreover, the metal is attached to the silica framework through a covalent bond, thus reducing the metal atoms' leaching during the reaction procedure.

Polyoxometalates have unparalleled physical and chemical properties due to their diverse structures and partial sizes [25, 26]. Polyoxometalates consists of a group of clusters of metals connected by oxygen. Muhammad reported that polyoxometalates can cover 6 to 368 metal ions in one molecule and that their size within the molecule can be controlled from several angstroms up to 10 nm [27, 28]. Keggin structures have the largest acidity among the solid acids and high catalytic activity [29]. Wells-Dawson solid acids are characterized by high selectivity in oxidation reactions.

In this work, MCM-41 (mobile composite material) was synthesized from rice husk residues and used as a support for cobalt substituted polyoxometalate ($H_8P_2W_{17}O_{61}Co(H_2O) \cdot 16H_2O$). The catalyst's acidity will be controlled by changing the $H_8P_2W_{17}O_{61}Co(H_2O) \cdot 16H_2O$ ratios deposited on the silica, MCM-41. The cracking efficiency of different catalysts was measured using a chemical probe (1,3,5-Triisopropylbenzene) into their initial moieties to identifying types of acid sites. The dodecane (represents gas oil model and one product of Fischer–Tropsch product) also be used to match the results of the TIPB probe cracking. The acidic site types were used in the interpretation of the obtained results..

2. Experimental

2.1 Materials

The rice husk used in this study was collected from the Kafr El-Sheikh governorate. sulfuric acid (95.0-98.0%), sodium hydroxide (≥97.0%, pellets), hydrochloric acid (36.5-38.0%), sodium tungstate dihydrate (≥99%), cobalt nitrate phosphoric acid (≥85 wt. % in H_2O), potassium chloride (99.5%), n-hexadecyltrimethylammonium bromide (95%), 1,3,5-triisopropylbenzene (95%), dodecane (≥99%), styrene (≥99%), toluene (99.8%), ethylbenzene (99.8%), 1,3-diisopropylbenzene (96%) were purchased from Sigma Aldrich.

2.2. Extraction of silica and sodium silicate from rice husk

_____

About 200 g of rice husk were previously cut and converted into small pieces and submitted into an autoclave (Parr -4848) adjective at 150 °C and 3 bars for 1 hr to remove the flux materials as alkaline metal oxides [30, 31]. After that, the rice husk was washed thoroughly with distilled water and dried overnight at 75 °C. Before calcination, the rice husk was treated with dilute sulfuric acid to prevent the formation of black silica after the calcination process. After neutralization and drying, the rice husk was calcined at 800 °C under airflow for 6 hr (the yield was ~13%). To prepare sodium silicate, 27 gm of the obtained silica was added to 100 gm of water containing 16 gm of sodium hydroxide under stirring. After 2 hr, the mixture was transferred to Teflon lined autoclave lined, and the mixture was heated to 120 °C for 8 hr. The soluble sodium silicate was filtered under a vacuum to remove solids.

2.3 Preparation of α-$K_6P_2W_{18}O_{62} \cdot 14H_2O$ and Co-substituted Heteropoly acids ($H_8P_2W_{17}O_{61}Co(H_2O)\cdot16H_2O$)

The α-$K_6P_2W_{18}O_{62}$ compound was prepared according to Mbomekalle [32]. Briefly, hydrochloric acid (200 ml, 0.4 M) was added to the sodium tungstate hydrate solution ($Na_2WO_4\cdot 2H_2O$, 260 g; 0.79 moles) under stirring for a period until the relatively cloudy solution becomes clear (this step was done to prepare ($[W_7O_{24}]^{6-}$). After that, another amount of hydrochloric acid (100 ml, 0.4 molars) and phosphoric acid (130 ml, 0.26 molar) were added simultaneously, and the stirring was continued until intense yellow appeared. After that, KCl (150 gm, 267 mol) was added to the yellow solution under vigorous stirring for 1 hr, and the precipitate was filtered off and dried under vacuum at 50 °C. The obtained compound was crystalline by hot water, where the material was boiled at 80 °C for a period of three days. After cooling and filtration, the obtained yellow crystal was 132 gm (62%).

The acid form of $H_8P_2W_{17}O_{61}Co(H_2O)\cdot16H_2O$ was prepared, according to Kharat et al., with slight modification [33]. $H_8P_2W_{17}O_{61}Co\cdot H_2O$ was prepared by dissolving 51 gm of $K_8P_2W_{18}O_{61}\cdot 15 H_2O$ in 200 ml hot water, and after completion of desolation, 3.36 gm of $Co(NO_3)_2$ dissolved in 40 ml of water was added under stirring for an hour. The resulting red color solution was cooled and extracted using diethyl ether and after vacuum removing of the solvent, the product crystallized in boiling with water for three days. Finally, the product was acidified with 140 ml hydrochloric acid (6 N), extracted by diethyl ether as a solvent, and dried under a vacuum at 50°C overnight.

2.4 Preparation of Tunable porous SiO₂-material and $H_8P_2W_{17}O_{61}Co(H_2O)$. 16 H₂O/SiO₂

The porous SiO_2 material was prepared following the hydrothermal method[34, 35]. n-hexadecyltrimethylammonium bromide (CTMABr; 13.2 g) was dissolved in 87 ml deionized water at 30 °C until a clear solution was obtained. After that, 11 ml of sodium silicate is added drop by drop to avoid gel formation under mechanical stirring. After the completion of the addition, the pH is adjusted to remain at 10 for 6 hours. The mixture was transferred to a stainless-steel autoclave lined with Teflon and conducting the hydrothermal process at 110 °C for a period of 48 hours. After self-cooling, the white precipitate was separated and washed with distilled water continuously to reach pH 6 and then dried at 80 °C. The material is subsequently calcined at 650 °C for 6 hours under a nitrogen atmosphere.

For the impregnation of $H_8P_2W_{17}O_{61}Co(H_2O)\cdot16H_2O$, the calcined SiO_2 material was suspended in deionized water. The quantities of $H_8P_2W_{17}O_{61}Co(H_2O)$. 16 H_2O required to be impregnated are 5, 10, and 15% on silica were dissolved in a warm distillate and added to the silica while stirring. After stirring for two hours, the water is removed by evaporation while stirring. The dried material is calcined at 450 ° C for 3 hours. The obtained materials were donated 5%CoHPA, 10%CoHPA, and 15%CoHPA, where the digits referred to the ratio of $H_8P_2W_{17}O_{61}Co(H_2O)\cdot16H_2O$.

2.5. Characterizations

X-ray diffraction spectroscopy of the prepared catalysts was performed by Bruker diffractometer using Cu-Kα (α = 1.54056 Å) at a scan rate of 3.0 sec-1 from 2θ of 10° to 80°. Potassium bromide has been used to prepare pellets of catalysts for FT-IR measurement using an FTIR-Bruker device. The prepared catalyst was exposed to pyridine-laden nitrogen at 70°C for 30 minutes; then, the excess pyridine was expelled by passing a stream of nitrogen over the catalyst at 90°C for 15 minutes. The obtained Brunauer–Emmett–Teller (BET) data of the prepared catalyst is from surface area analysis NOVA-touch device. The pore size distribution was calculated using the BJH method. The NH₃-TPD profile (temperature-programmed desorption of ammonia) was measured on BEL CAT device after removing adsorbed humidity.

2.6. Catalytic activity

2.6.1. 1,3,5-triisopropybenzene cracking

The catalytic cracking activity of the 1,3,5-triisopropybenzene compound on 5% CoHPA, 10% CoHPA, and 15% CoHPA catalysts was evaluated using a stainless steel fixed bed microreactor at temperatures ranging from 300 to 450 °C. The microreactor is attached to the preheating unit that is responsible for heating or vaporization 1,3,5-triisopropybenzene. The catalyst (1 gm) was packed after dilution with a similar percentage of quartz, and

_____

the diluted catalyst was supported by quartz wool, and a portion of the quartz wool was placed on top of the catalyst to distribute the feed on the catalyst surface. The catalyst was heating at 400 °C under nitrogen flow to get rid of moisture. A feed pump inserted Triisopropybenzene at WHSV of $1.5 \, hr^{-1}$, and the nitrogen/feed ratio was 50 ml min^{-1}. The cracking process products were analyzed using Agilent 7820A equipped with column HP-1 (100 m), TCD, and FID detectors. According to the outputs available from GC, the conversion of TIPP is determined using Eq. 1, while the selectivity of the products can also be identified according to Eq. 2

$$Conversion \, (\%) = \left(1 - \frac{mass \, of \, TIPB \, product}{mass \, of \, TIPB}\right) \quad (1)$$

$$Selectivity \, (\%) = \frac{mass \, fraction \, of \, each \, product}{mass \, fraction \, of \, total \, products} \quad (2)$$

2.6.2. *n*-Dodecane cracking

The catalytic cracking of the dodecane was accomplished in a fixed bed reactor. The reactor dimensions were 35 cm in length, the outer diameter and inner diameters were 8 cm and 5 cm, respectively, at four temperatures of 400, 450, 500, and 600 °C.This reactor is connected to a one-meter narrow tube heated at 260 °C to vaporize the dodecane molecules before reaching the catalyst. The reactor was filled with 5 cc catalyst loaded in the middle of the reactor with stable temperature. Small inert ceramic pieces fix the catalyst layer. Before performing the dodecane cracking process, it has been activated catalyst for 45 minutes at 400 °C under nitrogen flow at 150 ml min^{-1}. The dodecane feed was introduced to the preheated line at a constant flow (LHSV, liquid hourly space velocity, of $45 \, h^{-1}$) in the flow of helium gas (100 ml min^{-1}), which in turn was transferred to the main reactor. The reactor's output is attached to the preheated line at 220 °C connected to the TCD-FID GC device equipped with a capillary column, 100 meter HP-1 column. The conversion was obtained by changing the *n*-dodecane ratio

$$Conversion \, of \, n\text{-dodecane} \, (\%) = \left(1 - \frac{mass \, of \, n\text{-dodecane} \, product}{mass \, of \, n\text{-dodecane}}\right) \quad (3)$$

$$Selectivity \, to \, olefins \, (\%) = \frac{mass \, of \, olefin \, fraction}{mass \, fraction \, of \, total \, products} \quad (4)$$

3. Results and discussion

Fig 1a,b showed both the low and high-angle XRD results of SiO$_2$, 5%CoHPA, 10%CoHPA, and 15%CoHPA catalysts. For SiO$_2$, the peaks at 2θ = 2.2°, 4.2°, and 4.7° correspond to (100), (110), and (200) planes, demonstrating the hexagonal ordering structure of SiO$_2$materials (MCM-41). However, the *d$_{100}$* was decreased upon impregnation of

$H_8P_2W_{17}O_{61}Co(H_2O)\cdot16H_2O$ compound, suggesting more amount of $H_8P_2W_{17}O_{61}Co(H_2O)\cdot16H_2O$ impregnated on the hexagonal framework of SiO$_2$, which may cause damage to some extent to the ordered pore structure[26]. **Table 1** listed the pore characteristics of SiO$_2$ and 5%CoHPA, 10%CoHPA, and 15%CoHPA catalysts. It is clear that the unit cell parameter increase by increasing the CoHPA content may be due to the penetration of CoHPA in a silica framework or wall pore. Moreover, In the high angle XRD region (**Fig. 1b**), no peak was observed in CoHPA phases, indicating a high dispersion of CoHPA on the SiO$_2$ surface. The same behavior was documented on 20 wt.% HPW/MCM-41 by Zhao et al., [36], and the authors explained that due to the high dispersity of heteropoly acid on silica, MCM-41.

Nitrogen physisorption was performed as the essential estimation to analyze the structure of SiO$_2$ (MCM-41), 5%CoHPA, 10%CoHPA, and 15%CoHPA catalysts. If the prepared catalyst has a uniform or tunable pore diameter, the catalyst should reflect a perfect steepness due to the capillary condensation of nitrogen in the pore of SiO$_2$ support. As shown in (**Fig. 3),** all materials exhibit a sharp capillary condensation step, confirming highly ordered silica, 5%CoHPA, 10%CoHPA, and 15%CoHPA catalysts. However, the capillary condensation of 15%CoHPA catalyst seems somewhat less than other materials, maybe due to pores are somehow blocked by CoHPA material. The high adsorption volume of nitrogen of all catalysts demonstrates high surface area; the multipoint BET demonstrates the surface area is around 1170 m^2/g for pure SiO$_2$ and 1001, 903, and 852 m^2/g for 5%CoHPA, 10%CoHPA, and 15%CoHPA, respectively. The pore width figured by the BJH method was around 3.14 nm for all samples; however, the pore volume decreased directly with increasing the CoHPA ratio, as shown in (**Fig. 3d).**

To visualize the impact of the CoHPA compound on the morphology of SiO$_2$ materials. The parent SiO$_2$ support shows periodic pores ordering as parallel lines. The 5%CoHPA, 10%CoHPA, and 15%CoHPA catalysts images show a honeycomb-like structure (hexagonal pores array) with no visible aggregation of the CoHPA particle, which is good agreement with the low and high angle XRD analysis. However, as the CoHPA ratio increase to 15 wt, the uniform pores of SiO$_2$ material became invisible, suggesting the formation of a monolayer.

To know the location of a CoHPA particle or to ascertain the pore blockage effect of the CoHPA particle on SiO$_2$ as a host material, the normalized surface area (NS$_{BET}$) is conducted. The NS$_{BET}$ formula is expressed as [37, 38].

_____

$$NS_{BET} = \frac{SA_1}{1-y} \times \frac{1}{SA_2}$$

Where SA_1 is the surface area of CoHPA impregnated SiO_2, SA_2 is the surface area of SiO_2 and y is the mass fraction of CoHPA. When the obtained value of the NS_{BET} for the catalyst is nearest to 1, the CoHPA particles are very fine and located through both internal pores and the external surface. When the NS_{BET} is $\ll$ 1, " the CoHPA particles blocking the SiO_2 (MCM-41) pore located on the external surface. The calculation indicates that the NS_{BET} was 0.882, 0.812, and 0.783 for 5%CoHPA, 10%CoHPA, and 15%CoHPA, respectively, suggesting the presence of CoHPA particles in interior and exterior pores.

Fig.4a,b demonstrates the FTIR and pyridine-FTIR spectra of the calcined materials of SiO_2, 5%CoHPA, 10%CoHPA, and 15%CoHPA catalysts. The absence of the two sharp peaks at 2924 and 2852 cm^{-1} and their corresponding bending vibration at 1475 cm^{-1}is expected to the presence of C–H stretching of the hydrocarbon chain of the surfactant molecule confirm the complete removal of surfactant residue. The broad peak centered at 3450 cm^{-1} is ascribed to the stretching vibration of the hydroxyl group, while the low intense peak around 3195 cm^{-1} is assigned to surface silanols and adsorbed water particles [39]. The peak near 1615 cm^{-1} is attributed to the bending vibration of adsorbed water molecules. The asymmetric vibrations of Si–O–Si are seen at 1066 and 1228 cm^{-1}[40]. The peak at 952 cm^{-1}is ascribed to Si-OH vibrations. The peaks from 805 to 460 cm^{-1} have resulted from the bending vibration of the Si–O–Si bond, and the peak at 805 cm^{-1} may likewise relate to free SiO_2[41]. To better investigate the acidity of the prepared

materials, NH$_3$-TPD was utilized to quantify the quality and distribution of the different acid sites, as appeared in **Fig. 5.** The peaks in the scope of 86–170, 175–310, 315–470, and $\geq$470 °C are typically due to NH$_3$ chemisorbed on weak, medium Brønsted, strong Brønsted, and Lewis acid sites, respectively. Obviously, the concentration acid site contents are in order 15%CoHPA > 10%CoHPA >5%CoHPA, following the data obtained from the Pyr-FTIR spectroscopy. However, the 10%CoHPA sample has a more Brønsted acidity than the more ordering structure.

3.1. catalytic test
A. TIPB cracking

As to catalytic cracking of TIPB, it is settled that the cleavage of the propyl group from the benzene ring is the main reaction pathway from the benzene ring [42, 43]. Al-Khattaf et al. [44-47] detailed that the catalytic cracking of TIPB is a serious reaction. The TIPB compound is dealkylated to 1,3-DIPB (1,3-diisopropylbenzene) and propene, while the 1,3-DIPB delivered additionally experiences dealkylation to cumene and propene. The benzene and propene from the dealkylation of cumene speak to the third step of the response arrangement proposed. While the previously mentioned strides show up as the predominant ones, there are different responses, for example, disproportionation, isomerization, and condensation, that may influence gas stage item circulation and coke arrangement [42, 47]. Tsai et al. [48] detailed the degree to these products, which may rely on temperature and catalyst properties. The catalytic cracking of TIPB is accompanied by some different reactions, as outlined
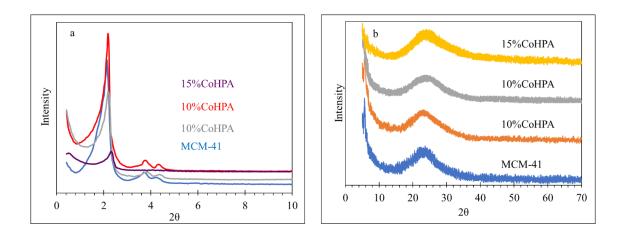
.

Fig.1. (a) low angle XRD and (b) wid angle XRD of the prepared catalyst

Table1. Surface Characterization of SiO2, 5%CoHPA, 10%CoHPA, and 15%CoHPA catalys

Catalysts	BET (m²/g)	Vp (cm3/g)	Dp (nm)	d100 (nm)	a0 (nm)	2θ (d100)	N$_{SBET}$
SiO₂	1170	0.86	3.24	4.123	4.761	2.14	
5%CoHPA	1001	0.801	3.21	4.047	4.673	2.18	0.882
10%CoHPA	903	0.754	3.17	4.011	4.631	2.2	0.812
15%CoHPA	852	0.721	3.14	3.77	4.354	2.34	0.783

Table 2. The product distribution of TIPB cracking over 5%CoHPA, 10%CoHPA, and 15%CoHPA catalysts

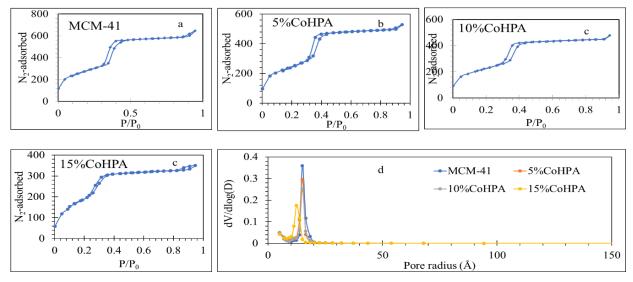| Sample	T (°C)	Time (mint)	conv. (%)	Gases	Tol.	Benz.	EB	Cum.	TMB	1,3-DIPB	2,4-DIPB	1,2-DIPB	Coke
5%CoHPA	300		19.75	7.8	0.09	2.5	0.31	2.1	0.89	4.4	0.9	0.24	0.52
10%CoHPA			31.76	11.6	0.32	4.1	0.12	1.9	0.2	7.3	5.01	0.23	0.98
15%CoHPA			42.84	21.1	0.21	8.6	1.03	3.2	1.33	2.3	3.49	0.27	1.31
5%CoHPA	350		21.98	8.6	0.1	2.9	0.25	2.7	1.1	4.2	1.1	0.14	0.89
10%CoHPA		30 min	33.44	13.4	0.45	5.1	0.19	2.3	0.42	6.7	3.73	0.17	0.98
15%CoHPA			43.67	19.82	0.15	9.4	0.83	5.4	1.02	2.8	2.92	0.23	1.1
5%CoHPA	400		24.83	9.5	0.3	3.4	0.22	3.9	1.4	3.4	1.2	0.01	1.5
10%CoHPA			36.05	14.6	0.6	6.9	0.22	4.1	0.5	5.2	1.94	0.14	1.85
15%CoHPA			51.79	16.42	2.22	4.9	3.17	5.6	6.86	6.3	2.29	1.43	2.6

Fig. 3. Nitrogen- adsorption isotherms and pore size distribution of SiO$_2$, 5%CoHPA, 10%CoHPA, and 15%CoHPA catalysts
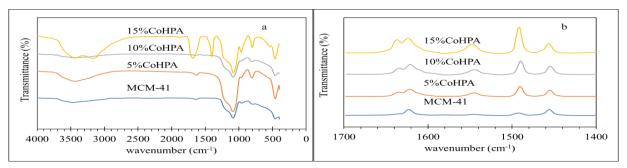
Fig.4a,b . FTIR and pyridine-FTIR spectra of the SiO$_2$ (MCM-41), 5%CoHPA, 10%CoHPA, and 15%CoHPA catalysts.

Table 3. The gas selectivity and percent of olefins in the products obtained from the TIPB cracking over 5%CoHPA,10%CoHPA, and 15%CoHPA catalysts

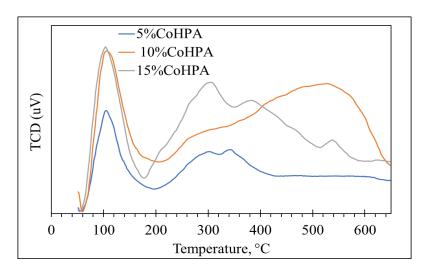| Sample	T(°C)	gases selectivity						C3=/C3	C4=/C4	iC4/C4
		C1+C2	C3	C3=	C4=	iC4	C4			
5%CoHPA		0.2	0.2	4.8	0.1	0.3	2.4	0.041	0.042	0.125
10%CoHPA	300	0.23	0.28	8.2	0.2	0.32	2.6	0.0341	0.077	0.123
15%CoHPA		0.53	0.6	15.3	0.45	1.3	3.5	0.0392	0.128	0.371
5%CoHPA		0.3	0.22	6.2	0.15	0.26	1.9	0.035	0.078	0.136
10%CoHPA	350	0.87	0.31	10.2	0.4	0.4	2.1	0.0303	0.192	0.191
15%CoHPA		0.63	0.63	16.5	0.5	0.45	2.2	0.0381	0.227	0.205
5%CoHPA		0.48	0.65	6.5	0.23	0.1	2.1	0.1	0.109	0.047
10%CoHPA	400	0.55	0.95	11.2	0.28	0.01	2.3	0.084	0.121	0.004
15%CoHPA		0.71	1.1	14.1	0.4	0.01	2.69	0.078	0.148	0.004

Fig.5. NH3 TPD patterns of of the 5%CoHPA, 10%CoHPA, and 15%CoHPA catalysts
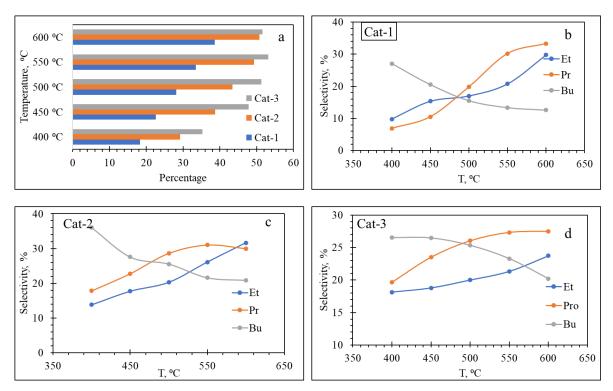
Fig. 6. (a) Dodecane conversion and (b-d) selectivity to olefins (Et = ethylene, Pr = propylene, and Bu = butene) at different temperatures over 5%CoHPA, 10%CoHPA, and 15%CoHPA catalyst

The primary items acquired from the reactant cracking of TIPB over 5%CoHPA, 10%CoHPA, and 15%CoHPA catalysts were benzene, cumene, diisopropylbenzenes, and propene (**Table 2**). Small measures of toluene, ethylbenzene, and trimethyl benzenes were additionally seen from the reaction products. These mixes (ethylbenzene, xylenes, and toluene) result from the cracking of the propyl group joined to the benzene ring [47, 49]. A most extreme TIPB transformation of ~40% was gotten at 400 °C after 30 min. The change of TIPB was seen to increment with response temperature. The conveyance of TIPB cracking items affirms the control of the three-stage arrangement responses proposed by Mahgoub and Al-Khattaf[50]. The yield of cumene and benzene expanded with reaction temperature, up to ~5.4%, and ~9.4%, individually, at 350 °C. As the temperature was additionally expanded to 400 °C, a slight increase in diisopropyl benzene yield was seen to estimate ~10% for 15%CoHPA catalysts. Meta-and para-diisopropyl benzene was recognized in the extensive sum over 5%CoHPA, 10%CoHPA, and 15%CoHPA catalysts due to the present loading of more amount HPA that cause some damage of the pore regularity of such materials, while a just decrease of ortho-diisopropyl benzenewas seen in the response items. The high measure of diisopropyl benzene seen in the catalytic cracking over 10%CoHPA and 15%CoHPA catalysts at 400 °C may be due to the presence of the Lewis acid site.

Table 3 demonstrates that the gases obtained from the catalytic cracking of TIPB at a different temperature. The methane, ethane, propane, isopropane, and butane are the most important items gotten in the reactant obtained over the 5%CoHPA, 10%CoHPA, and 15%CoHPA catalysts. It is clear that the gases are increased by increasing the temperature. However, the formed coke has affected this line. Additionally, the probability of saturated compounds is an interesting point the indicates that the Brønsted acid site is the main site for dealkylation, while the Lewis acid site is responsible for olefination [47].

B. Dodecane cracking

Fig. 6a shows the amount of n-dodecane conversion on 5%CoHPA, 10%CoHPA, and 15%CoHPA catalysts at temperatures in the 400 to 600 °C range. All of the catalysts showed the ability to crack n-dodecane into carbon numbers from C1 to C11; however, the selectivity toward definite carbon numbers is greatly differed due to the difference in the acidity of the catalyst. Using a temperature of 400°C, the n-dodecane conversion (%) was 37.7, 57.2, and 66.7 on 5%CoHPA, 10%CoHPA, and 15%CoHPA catalysts. The 10%CoHPA and 15%CoHPA catalysts showed high catalytic efficiency due to their higher acidity than the 5%CoHPAcatalyst. By raising the temperature to 600°C, the 5%CoHPA catalyst showed remarkable catalytic activity in the C-12 conversion, recording 67.9%, nearly twice the conversion at 400°C, while the 15%CoHPA catalyst showed a gradual C-12 conversion up to a temperature of 550°C, recording 86.7%. After that, the conversion rate of C-12 conversion 15%CoHPA catalyst decreased, which may be attributed to the formation of a high percentage of carbon on the catalyst's surface due to its high acidity.

The total distributions of the catalytic product were classified into paraffin and olefins, while aromatics and naphthenates were neglected due to the small amount produced. As shown in **Fig. 6a**, the olefins increase with increasing temperature, and its rate was the strongest using a Cat-3 catalyst. The Cat-1 achieved a regular increasing rate ratio of 18.3, 22.6, 28.1, 33.5, and 38.6% olefins at 400, 450, 500, 550, and 600 °C, respectively. The percentage of olefins obtained by Cat-2 was higher than Cat-1; however, the percentage difference was low at 550 and 600°C (43.4 and 49.3%). The Cat-3 catalyst achieved the highest percentage of olefins due to increasing the acidity of the catalyst, especially Lewis site, to reach the percentage of olefins to 53.2% at 550 °C, and the decline in olefins percentage at 600 °C may be due to the formation of coke. The selectivity towards carbon 2-4 olefins (ethylene, propylene, and butene) is shown in **Fig. 6b-d**, where it is clear that the selectivity towards short olefins increases with increasing temperature and that the Cat-2 shows good behavior, especially after the temperature exceeds 500 ° C. The selectivity of the prepared catalysts towards ethylene, propylene, and butene was somewhat different; for example, the Cat-1 catalyst showed an increase in selectivity towards ethylene with increasing temperature, where it achieved approximately 33%. The Cat-2 catalyst achieved a higher selectivity towards propylene production (31%) at 550 °C, while the selectivity output towards ethylene was about 31.2% at 600 °C. The selectivity towards butene decreases with increasing temperature, possibly due to a shift towards low molecular weight fractions. The Cat-3 catalyst achieved a low selectivity towards butene production in contrast to the other catalysts, but the decrease towards propane production was the least.

The sustainability aspect and circular economy

_____

sustainability is achieved byreducing the material consumption and depending on renewable resources. Therefore, as we mentioned before in this study,rice husk and silica were extracted from rice strawwhich is renewable and biodegradable so that the whole product is biodegradable. Also, the innovative model of circular economy requires maintaining the rate of products, materials and resources for as long as possible. These results are promising a great cost reduction as compared to the previously fabricated models.

Conclusion

Considering the economic factor in utilizing some wastes such as rice husk, silica was extracted from rice straw, converted to sodium silica in different percentages (5-15%). The analyses confirmed silica formation with tunable structure, which retained its tunability up to 10% loading rate, and the formation of pore disorder occurred at 15% loading. Ammonia-TPD analysis proved that the prepared catalysts possessed both Bronsted and Lewis acid sites, which had a good effect in cracking both TIPB and dodecane. The 10%CoHPA catalyst achieved the best catalytic activity because it has more Bronsted acid sites and well-tunability with less carbon surface formation. The selectivity of olefins as a required economic material was high as the catalyst achieved 38.6%.

.References

[1] B. Du, C. Chen, Y. Sun, M. Yu, M. Yang, X. Wang, J. Zhou, Catalytic conversion of lignin to bio-oil over PTA/MCM-41 catalyst assisted by ultrasound acoustic cavitation, Fuel Processing Technology, 206 (2020) 106479.

[2] B. Mallesham, D. Raikwar, D. Shee, The role of catalysis in green synthesis of chemicals for sustainable future, Advanced Functional Solid Catalysts for Biomass Valorization, (2020) 1.

[3] Y. Cao, S. Mao, M. Li, Y. Chen, Y. Wang, Metal/porous carbon composites for heterogeneous catalysis: old catalysts with improved performance promoted by N-doping, Acs Catalysis, 7 (2017) 8090-8112.

[4] O.O. Sadare, F. Obazu, M.O. Daramola, Biodesulfurization of petroleum distillates—current status, opportunities and future challenges, Environments, 4 (2017) 85.

[5] D.K. Ratnasari, M.A. Nahil, P.T. Williams, Catalytic pyrolysis of waste plastics using staged catalysis for production of gasoline range hydrocarbon oils, Journal of analytical and applied pyrolysis, 124 (2017) 631-637.

[6] R. Chal, C. Gérardin, M. Bulut, S. van Donk, Overview and Industrial Assessment of Synthesis Strategies towards Zeolites with Mesopores, ChemCatChem, 3 (2011) 67-81.

[7] R. Chal, C. Gérardin, M. Bulut, S. van Donk, Overview and industrial assessment of synthesis strategies towards zeolites with mesopores, ChemCatChem, 3 (2011) 67-81.

[8] S. Van Donk, A. Broersma, O. Gijzeman, J.A. van Bokhoven, J. Bitter, K. De Jong, Combined diffusion, adsorption, and reaction studies of n-hexane hydroisomerization over Pt/H–mordenite in an oscillating microbalance, Journal of Catalysis, 204 (2001) 272-280.

[9] D. Verboekend, G. Vilé, J. Pérez-Ramírez, Hierarchical Y and USY Zeolites Designed by Post-Synthetic Strategies, Advanced Functional Materials, 22 (2012) 916-928.

[10] A. Sachse, C. Wuttke, U. Díaz, M.O. de Souza, Mesoporous Y zeolite through ionic liquid based surfactant templating, Microporous and Mesoporous Materials, 217 (2015) 81-86.

[11] C. Manrique, A. Guzmán, J. Pérez-Pariente, C. Márquez-Álvarez, A. Echavarría, Vacuum gas-oil hydrocracking performance of Beta zeolite obtained by hydrothermal synthesis using carbon nanotubes as mesoporous template, Fuel, 182 (2016) 236-247.

[12] S.K. Mohamed, A.A. Ibrahim, A.A. Mousa, M.A. Betiha, , E.A. El-Sharkawy, H.M.A. Hassan, Facile fabrication of ordered mesoporous Bi/Ti-MCM-41 nanocomposites for visible light-driven photocatalytic degradation of methylene blue and CO oxidation, Separation and Purification Technology, 195 (2018) 174-183.

[13] H.M.A. Hassan, M.A. Betiha, R.F.M. Elshaarawy, M. Samy El-Shall, Promotion effect of palladium on Co 3 O 4 incorporated within mesoporous MCM-41 silica for CO Oxidation, Applied Surface Science, 402 (2017) 99-107.

[14] H.M.A. Hassan, S.K. Mohamed, A.A. Ibrahim, M.A. Betiha, E.A. El-Sharkawy, A.A. Mousa, A comparative study of the incorporation of TiO2 into MCM-41 nanostructure via different approaches and its effect on the photocatalytic degradation of methylene blue and CO oxidation, Reaction Kinetics, Mechanisms and Catalysis, 120 (2017) 791-807.

[15] M.S. Abdel Salam, M.A. Betiha, S.A. Shaban, A.M. Elsabagh, R.M. Abd El-Aal, F.Y. El kady, Synthesis and characterization of MCM-41-supported nano zirconia catalysts, Egyptian Journal of Petroleum, 24 (2015) 49-57.

[16] H.M.A. Hassan, E.M. Saad, M.S. Soltan, M.A. Betiha, I.S. Butler, S.I. Mostafa, A palladium(II) 4-hydroxysalicylidene Schiff-base complex anchored on functionalized MCM-41: An efficient heterogeneous catalyst for the epoxidation of olefins, Applied Catalysis A: General, 488 (2014) 148-159.

[17] A. Taguchi, F. Schüth, Ordered mesoporous materials in catalysis, Microporous and mesoporous materials, 77 (2005) 1-45.

[18] E. Antonakou, A. Lappas, M.H. Nilsen, A. Bouzga, M. Stöcker, Evaluation of various types of Al-MCM-41 materials as catalysts in biomass pyrolysis for the production of bio-fuels and chemicals, Fuel, 85 (2006) 2202-2212.

[19] D. Zhang, R. Wang, X. Yang, Beckmann rearrangement of cyclohexanone oxime over Al-MCM-41 and P modified Al-MCM-41 molecular sieves, Catalysis Communications, 12 (2011) 399-402.

[20] N.A. Fellenz, J.F. Bengoa, S.G. Marchetti, A. Gervasini, Influence of the Brönsted and Lewis acid sites on the catalytic activity and selectivity of Fe/MCM-41 system, Applied Catalysis A: General, 435-436 (2012) 187-196.

[21] K. Bachari, R. Chebout, R.M. Guerroudj, M. Lamouchi, Preparation and characterization of Zr-MCM-41 synthesized under microwave irradiation condition for acetylation of 1,2-dimethoxybenzene with acetic anhydride, Research on Chemical Intermediates, 38 (2012) 367-381.

_____

_____

[22] A.J. Koekkoek, J.R. van Veen, P.B. Gerrtisen, P. Giltay, P.C. Magusin, E.J. Hensen, Brønsted acidity of Al/SBA-15, Microporous and Mesoporous Materials, 151 (2012) 34-43.

[23] J.C. Bedoya, R. Valdez, L. Cota, M.A. Alvarez-Amparán, A. Olivas, Performance of Al-MCM-41 nanospheres as catalysts for dimethyl ether production, Catalysis Today, (2021).

[24] R.M. Martín-Aranda, J. Čejka, Recent Advances in Catalysis Over Mesoporous Molecular Sieves, Topics in Catalysis, 53 (2010) 141-153.

[25] D.L. Long, R. Tsunashima, L. Cronin, Polyoxometalates: building blocks for functional nanoscale systems, Angewandte Chemie International Edition, 49 (2010) 1736-1758.

[26] M.A. Betiha, H.M.A. Hassan, E.A. El-Sharkawy, A.M. Al-Sabagh, M.F. Menoufy, H.E.M. Abdelmoniem, A new approach to polymer-supported phosphotungstic acid: Application for glycerol acetylation using robust sustainable acidic heterogeneous-homogenous catalyst, Applied Catalysis B: Environmental, 182 (2016) 15-25.

[27] S. Liu, Z. Tang, Polyoxometalate-based functional nanostructured films: Current progress and future prospects, Nano Today, 5 (2010) 267-281.

[28] M. Genovese, K. Lian, Polyoxometalate modified inorganic–organic nanocomposite materials for energy storage applications: A review, Current Opinion in Solid State and Materials Science, 19 (2015) 126-137.

[29] R. Tayebee, F. Nehzat, E. Rezaei-Seresht, F.Z. Mohammadi, E. Rafiee, An efficient and green synthetic protocol for the preparation of bis (indolyl) methanes catalyzed by H6P2W18O62· 24H2O, with emphasis on the catalytic proficiency of Wells-Dawson versus Keggin heteropolyacids, Journal of Molecular Catalysis A: Chemical, 351 (2011) 154-164.

[30] V.P. Della, I. Kühn, D. Hotza, Rice husk ash as an alternate source for active silica production, Materials Letters, 57 (2002) 818-821.

[31] V.B. Carmona, R.M. Oliveira, W.T.L. Silva, L.H.C. Mattoso, J.M. Marconcini, Nanosilica from rice husk: Extraction and characterization, Industrial Crops and Products, 43 (2013) 291-296.

[32] I.-M. Mbomekalle, Y.W. Lu, B. Keita, L. Nadjo, Simple, high yield and reagent-saving synthesis of pure α-K6P2W18O62·14H2O, Inorganic Chemistry Communications, 7 (2004) 86-90.

[33] A.N. Kharat, P. Pendleton, A. Badalyan, M. Abedini, M.M. Amini, Oxidation of aldehydes using silica-supported Co(II)-substituted heteropolyacid, Journal of Molecular Catalysis A: Chemical, 175 (2001) 277-283.

[34] H. Zhu, R.V. Chaudhari, B. Subramaniam, A. Ramanathan, J.F. Wu, Effects of tunable acidity and basicity of Nb-KIT-6 catalysts on ethanol conversion: Experiments and kinetic modeling, AIChE Journal, (2017).

[35] C. Sener, T. Dogu, G. Dogu, Effects of synthesis conditions on the structure of Pd incorporated MCM-41 type mesoporous nanocomposite catalytic materials with high Pd/Si ratios, Microporous and mesoporous materials, 94 (2006) 89-98.

[36] Z. Zhao, Y. Dai, T. Bao, R. Li, G. Wang, Direct alkenylation of aromatics with phenylacetylene over supported H3PW12O40 catalysts as a clean and highly efficient approach to producing α-arylstyrenes, Journal of Catalysis, 288 (2012) 44-53.

[37] L. Vradman, M. Landau, D. Kantorovich, Y. Koltypin, A. Gedanken, Evaluation of metal oxide phase assembling mode inside the nanotubular pores of mesostructured silica, Microporous and mesoporous materials, 79 (2005) 307-318.

[38] M. Betiha, A. Rabie, A. Elfadly, F. Yehia, Microwave assisted synthesis of a VO x-modified disordered mesoporous silica for ethylbenzene dehydrogenation in presence of CO 2, Microporous and Mesoporous Materials, 222 (2016) 44-54.

[39] M. Popova, A. Szegedi, P. Németh, N. Kostova, T. Tsoncheva, Titanium modified MCM-41 as a catalyst for toluene oxidation, Catalysis Communications, 10 (2008) 304-308.

[40] M.M. Ambursa, P. Sudarsanam, L.H. Voon, S.B.A. Hamid, S.K. Bhargava, Bimetallic Cu-Ni catalysts supported on MCM-41 and Ti-MCM-41 porous materials for hydrodeoxygenation of lignin model compound into transportation fuels, Fuel Processing Technology, 162 (2017) 87-97.

[41] P. Monash, G. Pugazhenthi, Investigation of equilibrium and kinetic parameters of methylene blue adsorption onto MCM-41, Korean Journal of Chemical Engineering, 27 (2010) 1184-1191.

[42] A. Corma, B. Wojciechowski, The catalytic cracking of cumene, Catalysis Reviews Science and Engineering, 24 (1982) 1-65.

[43] M.A. Betiha, H.M. Hassan, A.M. Al-Sabagh, S.K. Abd El Rahman, E.A. Ahmed, Direct synthesis and the morphological control of highly ordered mesoporous AlSBA-15 using urea-tetrachloroaluminate as a novel aluminum source, Journal of Materials Chemistry, 22 (2012) 17551-17559.

[44] J. Atias, G. Tonetto, H. De Lasa, Catalytic conversion of 1, 2, 4-trimethylbenzene in a CREC riser simulator. A heterogeneous model with adsorption and reaction phenomena, Industrial & engineering chemistry research, 42 (2003) 4162-4173.

[45] S. Al-Khattaf, H. De Lasa, The role of diffusion in alkyl-benzenes catalytic cracking, Applied Catalysis A: General, 226 (2002) 139-153.

[46] M.A. Betiha, M.F. Menoufy, A.M. Al-Sabagh, H.M. Hassan, S.A. Mahmoud, Acidic mesostructured aluminosilicates assembled from economic acidic template characterized by catalytic cracking reactions, Microporous and Mesoporous Materials, 204 (2015) 15-24.

[47] H.M. Hassan, M.A. Betiha, S.K. Abd El Rahman, M. Mostafa, M. Gallab, Hafnium pentachloride ionic liquid for isomorphic and postsynthesis of HfKIT-6 mesoporous silica: catalytic performances of Pd/SO42−/HfKIT-6, Journal of Porous Materials, 23 (2016) 1339-1351.

[48] L.-Y. Fang, S.-B. Liu, I. Wang, Enhanced para-selectivity by selective coking during toluene disproportionation over H–ZSM-5 zeolite, Journal of Catalysis, 185 (1999) 33-42.

[49] T. Odedairo, R. Balasamy, S. Al-Khattaf, Influence of mesoporous materials containing ZSM-5 on alkylation and cracking reactions, Journal of Molecular Catalysis A: Chemical, 345 (2011) 21-36.

[50] K. Mahgoub, S. Al-Khattaf, Catalytic cracking of hydrocarbons in a riser simulator: the effect of catalyst accessibility and acidity, Energy & fuels, 19 (2005) 329-338.

_____